

Onset of turbulence in channel flows with scale-invariant roughness

Gaute Linga ^{1,2,*} Luiza Angheluta ¹ and Joachim Mathiesen ^{1,2}

¹*PoreLab, The Njord Centre, Departments of Physics and Geosciences, University of Oslo, P.O. Box 1048, NO-0316 Oslo, Norway*

²*Niels Bohr Institute, University of Copenhagen, Blegdamsvej 17, DK-2100 Copenhagen, Denmark*



(Received 3 July 2020; accepted 15 June 2022; published 29 July 2022)

Using 3D direct numerical simulations of the Navier–Stokes equations, we study the effect of a self-affine wall roughness on the onset of turbulence in channel flow. We quantify the dependence of the turbulent intensity (proportional to the mean-squared velocity fluctuations) on the Reynolds number Re for different roughness amplitudes A . We find that for sufficiently high amplitudes, $A > A_b$, the transition changes its nature from being subcritical (as is known at $A = 0$) to supercritical, i.e., the boundary roughness renders the flow unstable for $Re > Re_l$, where the critical Re_l decays nontrivially with increasing A . The dependence of the friction factor on Re is found to follow a generalized Forchheimer law, which interpolates between the laminar and inertial asymptotes. The transition between these two asymptotes occurs at a second critical Re_c which is comparable in magnitude to Re_l . This implies that transitional flow is an integral part of flow in open fractures when Re is sufficiently high, and should be accounted for in effective modeling approaches.

DOI: [10.1103/PhysRevResearch.4.033086](https://doi.org/10.1103/PhysRevResearch.4.033086)

I. INTRODUCTION

Since the early experiments by Reynolds [1], the onset of turbulence in wall-bounded flows has been an open problem in fluid dynamics with recent breakthroughs in our understanding of the flow between smooth walls [2–5]. In the smooth-wall limit, the onset of turbulence is via a subcritical transition, meaning that the laminar state is linearly stable and nonlinear perturbations are necessary in order to produce proliferation of self-sustained velocity fluctuations. These localised turbulent structures spread or decay and fill the system through spatiotemporal intermittency. Recently, the subcritical transition in flows bounded by smooth walls has been connected to the directed percolation phase transition, and is generally thought to belong to the same universality class [6–12]. Much less is known about the nature of the onset to turbulence in the presence of wall roughness. The classical Nikuradse measurements [13] of the friction factor in pipe flows with discrete wall asperities remain the main benchmark in this field, and most efforts have focused on the high Reynolds number (Re) regime rather than the transitional regime [14]. Recent work [15,16] has reported that the addition of a sufficient amount of particles to pipe flows may render the laminar base flow unstable and the transition to turbulence as supercritical, directly passing to turbulence without spatiotemporal intermittency.

In this paper, we present a systematic study on the transition to turbulence in 3D flows bounded by rough walls that have a continuous and self-affine roughness. This can be considered as a prototypical, minimal model for flow in fractured materials. Although flow in open fractures has been extensively studied, most computational work has been done in the low Re regime [17–19] or for steady state flows [19–22]. In contrast, unsteady flow in open fractures is much less studied and understood [18,20], hence its impact on macroscopic transport properties remain elusive, particularly around the turbulent transition point. For instance in Ref. [18], the authors simulated high-velocity flow in a self-affine fracture joint, and found that the relationship between average forcing f and mean flow u_x was well described by a cubic form [23,24], $f \sim u_x + ku_x^3$ (k being an empirical constant) at low Re , and the empirical Forchheimer law,

$$f = au_x + bu_x^2, \quad (1)$$

at higher Re (a, b are empirical coefficients). However, the assumption of a 2D, time-independent flow field precluded a realistic resolution of turbulent or transitional flows, which we, in this paper, will show is necessary.

Using 3D direct numerical simulations (DNS) of the time-dependent Navier–Stokes equations, we characterize the transition to turbulence in channels with self-affine boundary roughness (the model system and equations are described in Sec. II). By looking at the turbulent intensity, defined to be proportional to the mean-square fluctuations, we show that the transition to turbulence changes its nature from subcritical to supercritical for sufficiently large roughness amplitude (Sec. III). Furthermore, we determine robust scaling behavior of friction factor with Re and roughness amplitude in the steady and time-dependent transitional regimes (Sec. IV). Based on our simulations, we sketch a phase diagram of the

*gaute.linga@mn.uio.no

transition (Sec. V) and discuss implications and limitations of our results (Sec. VI).

II. GOVERNING EQUATIONS AND SYSTEM SETUP

As a simple idealisation of open fracture, we consider two identical self-affine surfaces that are shifted vertically along the z axis by a fixed distance d . They form a channel which is periodic in the x and y in-plane directions. This type of geometry is known as a fracture joint, resulting from mode I fracture, in contrast to a fault, where the surfaces would be shifted both vertically and in the xy plane [18]. The self-affine fracture surface denoted as a $z = h(x, y)$ [25] is a random surface that is statistically invariant under the scale transformation $(x, y, z) \rightarrow (\lambda x, \lambda y, \lambda^H z)$, [26,27]. Here, H is the Hurst exponent, which we set to $H = 0.8$, representative for most fractures in 3D [28,29].

We define the *roughness amplitude* as the root-mean-square height deviation, $A = L^{-1}(\int_0^L \int_0^L h^2(x, y) dx dy)^{1/2}$. Due to the self-affine nature of the surface, the amplitude scales with the system size as $A \sim L^H$. We therefore expect that the flow properties dependent on the roughness amplitude will also indirectly scale nontrivially with the system size. This has been investigated in the lubrication approximation (see e.g., [30]), but is computationally much more challenging to do in 3D DNS. Due to the inherent computational complexity, we limit our study to a fixed size L . The roughness amplitudes have been chosen to be $A \in \{0, 0.1d, 0.2d, 0.5d, 0.8d\}$, as compared to the channel width $d = 1$.

We perform DNS of the incompressible Navier–Stokes equations,

$$\partial_t \mathbf{u} + \mathbf{u} \cdot \nabla \mathbf{u} - \nu \nabla^2 \mathbf{u} = \frac{1}{\rho} (-\nabla p + \mathbf{f}), \quad (2)$$

$$\nabla \cdot \mathbf{u} = 0, \quad (3)$$

in a channel with self-affine walls using a finite element method and unstructured tetrahedral meshes [31] (see the Supplemental Material [32] for details on numerical implementation). Here \mathbf{u} is the velocity field, ν is the kinematic viscosity, ρ is the constant density, and p is the pressure. The flow is driven by a constant, uniform body force $\mathbf{f} = f \hat{\mathbf{e}}_x$, where $\hat{\mathbf{e}}_x$ is the streamwise direction, either to a laminar or a transitionally turbulent flow depending on the magnitude of \mathbf{f} . The force \mathbf{f} is in the steady state (where the velocity is *at*, or temporally fluctuating around, a constant value) compensated by the friction between the flow field and the rough walls. At the same time it controls the injected energy per time, $\int_{\Omega} \mathbf{f} \cdot \mathbf{u} dV$ (V is volume), which is compensated by the (turbulent or laminar) dissipation rate, both at the walls and in the bulk. We quantify our results using the flux-based Reynolds number $\text{Re} = \langle u_x \rangle d / \nu$, where $u_x = \mathbf{u} \cdot \hat{\mathbf{e}}_x$ is the streamwise velocity, here the overbar is the time average and $\langle \cdot \rangle$ is the spatial integral over the computational domain.

In all simulations, no-slip conditions are applied at the boundaries, $\mathbf{u} = \mathbf{0}$ for $\mathbf{x} \in \partial\Omega$. We have also made sure that our results are insensitive to whether we start simulations from below, i.e., either at $\text{Re} = 0$ or from a steady laminar or a transitional state below the sought Re , or above.

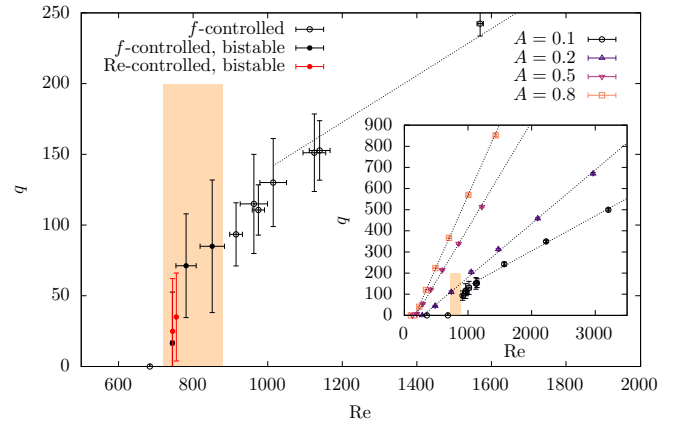


FIG. 1. The fluctuation strength q (indicator of turbulence) as a function of the Reynolds number Re . The main panel shows a zoom-in at the near-critical region for roughness amplitude $A = 0.1$. The shaded region indicates the region where a bistable behavior is observed. Both the standard force-controlled (f -controlled) simulations and two flux-controlled (Re-controlled) simulations are included. The inset shows q for all considered roughness amplitudes A , except the bistable region for visual clarity. Only force-controlled simulations are included in the inset. The absolute size of the shaded region is the same in both panels.

III. NATURE OF THE ONSET TO TRANSITIONAL FLOWS

We discern between *steady* (laminar) flow and unsteady flow, which can in principle mean both time-periodic laminar flow (where there is essentially no nonlinear transfer of energy across scales) or turbulent flow. However, we assume that for flow over a sufficiently large rough surface (with high enough amplitude to produce detaching vortices), a time-periodic signal from a single defect will not contribute significantly to the overall transport properties. Above this, there will be several (for an infinitely large domain, infinitely many) interacting “defects” that produce vortices, and thus no time-periodic signal should be found. By using Reynolds decomposition, the velocity field $\mathbf{u}(\mathbf{x}, t)$ can be decomposed into its *expectation value* $\bar{\mathbf{u}}(\mathbf{x})$ and the *velocity fluctuations* $\mathbf{u}'(\mathbf{x}, t)$, i.e., $\mathbf{u}(\mathbf{x}, t) = \bar{\mathbf{u}}(\mathbf{x}) + \mathbf{u}'(\mathbf{x}, t)$.

We measure flow fluctuations by the strength of the root-mean-square velocity variations. We define the dimensionless quantity which measures the strength of fluctuations as

$$q(\text{Re}, A) = \frac{\sqrt{\langle |\mathbf{u}'(\mathbf{x}, t)|^2 \rangle} d}{\nu},$$

which depends on the Re number and roughness amplitude. This quantity is zero in the laminar state and nonzero near and above the onset of unsteady flow, and thus can be used as a global order parameter for the transition to unsteady flows.

In the inset of Fig. 1, we show the dependence of q on Re for all simulated roughness amplitudes A . For sufficiently high Re , the data for all roughness amplitudes obey linear relationships. For $A = 0$, it is well known that the transition to turbulence is subcritical, which in a finite system would manifest as a discontinuous jump in the order parameter (see [33,34]). However, for high roughness amplitudes, $A > 0.1$, the linear relationships extend all the way down to $q = 0$. This

implies that the flow is linearly unstable, i.e., that any perturbation away from a stationary velocity profile will grow. Thus, unsteady flow is continuously produced by the boundary for $\text{Re} > \text{Re}_l$, where Re_l is a *first* critical Re which quantifies the point where *transitional flow* sets in. Based on the adequacy of linear fits (as outlined above) to describe the $q(\text{Re})$ data over roughly an order of magnitude, we propose the following relation for each amplitude A :

$$q(\text{Re}) = \begin{cases} 0 & \text{for } \text{Re} < \text{Re}_l, \\ k_q(\text{Re} - \text{Re}_l) & \text{for } \text{Re} \geq \text{Re}_l, \end{cases} \quad (4)$$

which holds for amplitudes $A \gtrsim 0.2$. Here, both the proportionality coefficient k_q and Re_l depend only on A . The dependence of Re_l on A is nontrivially decaying and shown in Fig. 3.

For the lowest nonzero amplitude investigated, $A = 0.1$, the linear relationship does not extend down to $q = 0$, and instead there seems to be jump consistent with a subcritical transition (as for $A = 0$). However, upon closer inspection shown in the main panel of Fig. 1, the transition is indeed continuous but curves sharply towards $q = 0$ for $\text{Re} \simeq 750$, meaning that the flow is still linearly unstable at this (Re, A) . The vertical “error bars” show the standard deviation in the time signal for the instantaneous turbulent intensity, i.e., $q_t(t) = \sqrt{\langle |\mathbf{u}'|^2(t) \rangle} d/\nu$, and are seen to increase closer to the transition. This indicates the presence of metastable turbulent structures whose intensity varies strongly in time. In particular, it reflects the bistable flow dynamics that we observe close to the transition (indicated in Fig. 1): relatively long periods of almost quiescence (slow buildup) interrupted by short durations of turbulence that fills the whole system and quickly decays to restart the buildup. Further, the horizontal “error bars”, which show the standard deviation in the instantaneous Reynolds number $\text{Re}_t = \langle \mathbf{u} \cdot \hat{\mathbf{x}} \rangle d/\nu$, also increase close to the transition. To rule out whether the variations in the global flow rate is what mainly contributes to q and its fluctuations, we have carried out a set of simulations with fixed flow rate (i.e., Re -controlled simulations, cf. Fig. 1; see Supplemental Material [32] for details). The results are consistent with the standard, force-controlled (f -controlled, cf. Fig. 1) simulations, strengthening the notion that the transition is indeed supercritical even at amplitude $A = 0.1$. However, for this A there exists an interval in Re where turbulent structures that would otherwise decay are retriggered by the boundary defects. This is not the case for $A > 0.2$ where there is no sign of bistability: once the base flow becomes linearly unstable, turbulence starts to fill the bulk of the system.

IV. FRICTION FACTOR

We define a dimensionless *geometrical friction coefficient*,

$$C_f = \frac{fd^2}{12\nu\langle u_x \rangle}, \quad (5)$$

which is a dimensionless measure of the hydraulic resistance of the channel [22] (see the discussion of different definitions in Appendix B). In Fig. 2, we present a diagram of the statistical steady-state relationship between Re and the friction factor C_f for the various roughness amplitudes. For low Re , C_f attains a constant value $C_{f,0}$ dependent on the roughness A ,

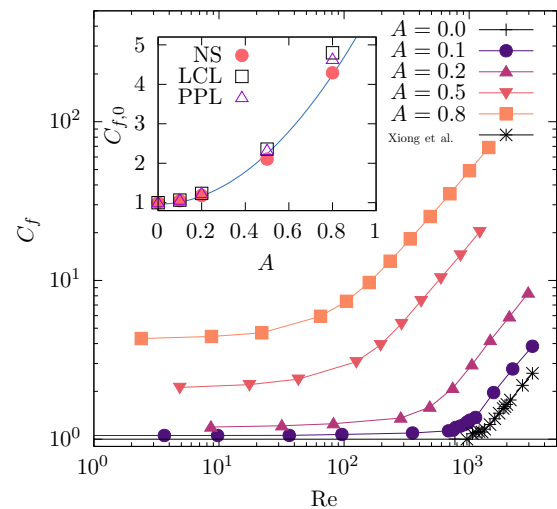


FIG. 2. Friction factor C_f plotted against Reynolds number Re for the five roughness amplitudes A . The data for PPF marked with star symbols are taken from Xiong *et al.* [35]. Inset: Purely geometric contribution to the friction factor, i.e., $C_{f,0} = C_f(\text{Re} \rightarrow 0)$. The numerical simulations using the Navier–Stokes equations (NS) are compared to the parallel plate law (PPL) and the local cubic law (LCL), which yields reasonable agreement. A parabolic fit to the simulation data (blue line) is shown as a guide to the eye.

whereas at higher Re , there is a crossover where C_f increases linearly with Re . As shown in the inset of Fig. 2, the purely geometric friction factor $C_{f,0}$ is well predicted by the local cubic law based on local effective apertures (see Supplemental Material [32]), and the parallel plate law based on mean aperture. However, the crossover between the two regimes, where the flow becomes non-laminar and the inertial effects begin to take over, cannot be predicted from $C_{f,0}$ alone. By fitting the data in Fig. 2 to a generalized Forchheimer equation (see Appendix A),

$$\frac{C_f}{C_{f,0}} = \left[1 + \left(\frac{\text{Re}}{\text{Re}_c} \right)^\beta \right]^{1/\beta}, \quad (6)$$

we identify a *second* critical Reynolds number Re_c indicating where nonlinear effects become important for the friction factor. This is in contrast to Re_l which quantifies the point where the base flow becomes linearly unstable. Similarly to $\text{Re}_l(A)$, the dependence of Re_c on A is decaying and shown in Fig. 3. The other parameters in Eq. (6) are discussed in Appendix A.

V. COMPARISON BETWEEN CRITICAL REYNOLDS NUMBERS AND A PHASE DIAGRAM OF THE TRANSITION

In Fig. 3, the two critical Reynolds numbers Re_l and Re_c found in this work (and for the $A = 0$ case, in the literature [36]) are compared. Additionally, we superimpose a third critical Re , Re_\times , found in the literature [37]. Re_\times corresponds to the Re where an isolated turbulent structure is equally likely to spread as to decay, which underpins the statistical nature of the transition [38]. The value of Re_\times is only estimated for $A = 0$ and, to guide the eye, it is extrapolated by a constant

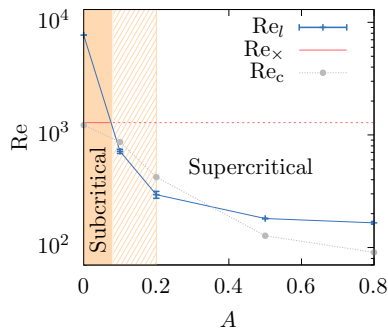


FIG. 3. Comparison of different critical Reynolds numbers Re for varying roughness amplitude A . The critical Re for linear stability, Re_l , is based on literature ($A = 0$ from [36]) and our measurements of q ($A \geq 0.1$). The critical Re for the statistical transition to turbulence, Re_x , is only available at $A = 0$ [37] and is extrapolated as a constant to guide the eye. The critical Re for the transition between the two scalings of the friction factor, Re_c , is superimposed and qualitatively follows the lower of Re_l and Re_x . In the figure, we have also sketched the interval in A where the transition is subcritical (orange shade) and supercritical (white shade). The hashed region indicates where the transition goes from being subcritical (through supercritical bistable) to supercritical.

for finite A . Using these curves it is possible to sketch a phase diagram of the turbulent transition in rough channels. When $Re_x < Re_l$, that is, for amplitudes $A < A_b$ where the bifurcation amplitude A_b is slightly below 0.1, the transition is subcritical. It is hard to give a more precise estimate of A_b due to the lack of data for Re_x for $A > 0$. For $A > A_b$, the base flow is linearly unstable and the transition is supercritical. However, for a limited range of $A < 0.2$ the flow is in a bistable state, as discussed in Sec. III.

We also note from Fig. 3 that Re_c , associated with the change in the scaling of C_f , trails the lowest of Re_l and Re_x . In particular, there is only a narrow range, $Re \in [Re_c, Re_l]$ (for sufficiently high A), where the flow is time independent and where simultaneously C_f departs significantly from $C_{f,0}$.

VI. DISCUSSION AND CONCLUSION

In this paper, we have investigated the transition to turbulence in self-affine channels representative of open fractures, and quantified its effect on the friction factor. One major advancement of this study compared to previous ones is that we focus on time-dependent transitional flow for various roughness amplitudes. Our main result is that the nature of the transition changes character at a given roughness amplitude $A = A_b$ which we estimate to be slightly below 0.1. In particular, by inspecting the turbulent intensity q (mean-square velocity fluctuations), we show that the transition goes from being subcritical, as is known for smooth walls ($A = 0$), to being subcritical at sufficiently high A . For values of A slightly above A_b , the transition has a bistable character where the flow varies between slow build-up and quick decay of domain-filling turbulence.

We found that self-affine wall roughness has significant impact on the macroscopic flow properties. The critical Re

number Re_c where inertial effects come into play decreases monotonously with A in a similar manner as Re_l , consistently with our understanding of roughness-induced turbulence. The observation that Re_c and Re_l have a comparable magnitude and dependence on A , implies that there is only a narrow region in $Re \in [Re_c, Re_l]$ where inertial effects are present but where the flow remains laminar. For effective modeling approaches aiming to use friction factor correlations, this implies that turbulent effects must be accounted for when estimating transport processes such as mixing, dispersion, and heat transfer even at moderate Re . The crossover region from the constant asymptote, $C_f \sim C_{f,0}$ for $Re \ll Re_c$, to the linear asymptote $C_f \sim Re$ for $Re \gg Re_c$, can be described by a generalised Forchheimer equation (6). The purely geometric friction factor $C_{f,0}$ scales approximately quadratically with the roughness amplitude A . For future work, it would be interesting to investigate the applicability of this description to other geometries and whether it could be justified on more rigorous grounds.

It is also important to emphasise the current computational limitations associated with this problem. At present, we consider a single realisation of a self-affine surface and varied only the roughness amplitude. A more quantitative analysis will require taking ensemble averages of many realisations of self-affine surfaces and other types of roughness (e.g. Nikuradse-type roughness [13,39]). A consequent limitation relates to the system size, which in our simulations is fixed to $L = 10d$. As a comparison, the length scale of the domain considered in a recent study of Waleffe (simplified Navier–Stokes) flow [33] was roughly equivalent to $L \simeq 1280d$ (in our units). Such domain sizes are out of reach with the finite element method used here.

It is known that transport properties of self-affine channels scale nontrivially with the system size [30]. Thus, further studies are needed for variable system sizes to better understand how the scaling behavior of friction factors and the sub- and supercritical transitions depend on the system size. Furthermore, it is an open question how the bistability observed at moderate A depends both on the system size and on the particular realization of a self-affine surface. A possible route to achieving large system sizes with reduced computational cost compared to the finite element method used here might be to follow in the lines of Ref. [40]. Here, instead of resolving the complex boundary directly, an effective body force was used to model boundary friction [41]. However, this way of modeling roughness cannot produce vortices that are released into the bulk, and will thus be unrealistic when the roughness amplitude is sufficiently large.

ACKNOWLEDGMENTS

The authors thank Anier Hernandez-Garcia and Mads H. A. Madsen for helpful discussions. This project has received funding from the European Union’s Horizon 2020 research and innovation program through Marie Curie initial training networks under Grant Agreement No. 642976 (ITN NanoHeal), and from the Research Council of Norway through its centers of Excellence funding scheme, Project No. 262644 (PoreLab), and through Project No. 325819 (M4).

APPENDIX A: UNIFIED DESCRIPTION OF THE FRICTION FACTOR AND ITS CROSSOVER REYNOLDS NUMBER Re_c

In order to quantify the crossover in Re , we consider the functional form Eq. (6) as a good fit to the entire range of data, at each roughness. Here, $C_{f,0}$ is the purely geometric friction factor, identified in the limit $Re \rightarrow 0$, while Re_c is a critical Re number where the inertial effects come into play. The exponent β in Eq. (6) controls the width of the transition region between the two regimes; a high (low) exponent indicates a narrow (broad) region. Note also that when $\beta \rightarrow \infty$, $C_f/C_{f,0} = \max(1, Re/Re_c)$. When $\beta = 1$, Eq. (6) is consistent with the Forchheimer law (1) (see also Section B and Eq. (B2) for an alternative formulation). Further, when $\beta = 2$, Eq. (6) attains a quadratic correction term for $Re/Re_c \ll 1$, which is consistent with the weak inertia law. It is thus clear that Eq. (6) can be seen as a generalized Forchheimer equation. While Eq. (6) does not have a direct physical motivation, it describes the data well and provides an unbiased determination of Re_c for all roughness amplitudes A . $C_{f,0}$ can be read off directly from the simulation data in the $Re \simeq 0$ limit, which means that β and Re_c can be considered as the only two fitting parameters in the expression, and are readily calculated using a nonlinear least squares method.

A final test of the unified description of the data presented in Fig. 2 is to inspect how well they collapse when rescaled by the parameters $C_{f,0}$ and Re_c . In Fig. 4, we plot for all simulated roughness amplitudes A , $C_f/C_{f,0}$ as a function of Re/Re_c . For all A , the data is seen to follow the same asymptotic behavior, differing only in the transition region (which in the least squares fit was captured by β). In particular, the transition region becomes wider as the roughness is increased, consistent with the quantitative observation of the behavior of $\beta(A)$, shown in the inset of Fig. 2.

APPENDIX B: DEFINITIONS OF THE FRICTION FACTOR

We choose the definition Eq. (5) of C_f , because for Stokes flow ($Re \rightarrow 0$), this $C_f = C_{f,0}$ comes out as a purely geomet-

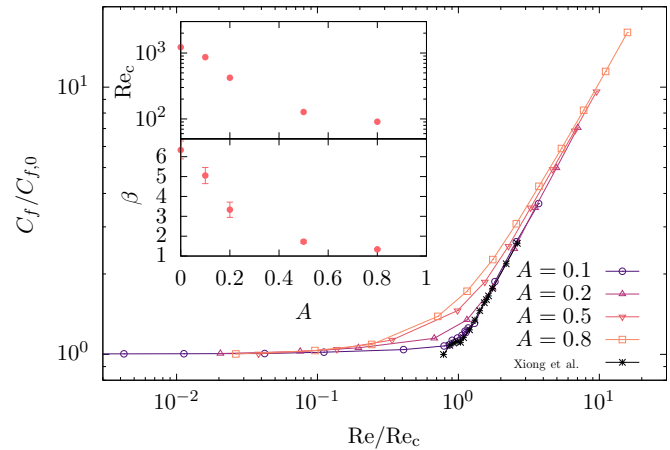


FIG. 4. Data collapse of the scaled geometric friction factor, $C_f/C_{f,0}$, as function of Re/Re_c for all roughness amplitudes A considered in the present work (replotted data of Fig. 2). The insets show two fitted parameters using Eq. (6) ($C_{f,0}$).

ric quantity. The prefactor $1/24$ is chosen such that $C_f = 1$ for plane Poiseuille flow (i.e., $A = 0$).

Another commonly applied quantity (especially for pipe flows) is the Darcy friction factor f_D , defined through the Darcy–Weisbach relation $f_D = f d / (\frac{1}{2} \langle u_x \rangle^2)$. These two quantities are related to each other by

$$C_f = \frac{f_D Re}{24}. \tag{B1}$$

For the special case of laminar flow between two parallel plates (PPL), we thus have $f_D = 24/Re$.

Using Eq. (B1), Eq. (6) can be written in terms of the Darcy friction factor as

$$\frac{f_D}{f_{D,\infty}} = \left[\left(\frac{Re_c}{Re} \right)^\beta + 1 \right]^{1/\beta}, \tag{B2}$$

which attains the qualitatively correct asymptotes $f_D \sim Re^{-1}$ for $Re \ll Re_c$, and $f_D \sim f_{D,\infty} = \text{const.}$ for $Re \gg Re_c$, cf. [42, Eq. (5)]. The asymptote is then given by $f_{D,\infty} = 24C_{f,0}/Re_c$.

[1] O. Reynolds, An experimental investigation of the circumstances which determine whether the motion of water shall be direct or sinuous, and of the law of resistance in parallel channels, *Phil. Trans. R. Soc.* **174**, 935 (1883).
 [2] K. Avila, D. Moxey, A. de Lozar, M. Avila, D. Barkley, and B. Hof, The onset of turbulence in pipe flow, *Science* **333**, 192 (2011).
 [3] D. Barkley, B. Song, V. Mukund, G. Lemoult, M. Avila, and B. Hof, The rise of fully turbulent flow, *Nature (London)* **526**, 550 (2015).
 [4] D. Barkley, Theoretical perspective on the route to turbulence in a pipe, *J. Fluid Mech.* **803**, P1 (2016).
 [5] V. Mukund and B. Hof, The critical point of the transition to turbulence in pipe flow, *J. Fluid Mech.* **839**, 76 (2018).
 [6] N. Goldenfeld, Roughness-Induced Critical Phenomena in a Turbulent Flow, *Phys. Rev. Lett.* **96**, 044503 (2006).
 [7] N. Goldenfeld and H.-Y. Shih, Turbulence as a problem in non-equilibrium statistical mechanics, *J. Stat. Phys.* **167**, 575 (2017).
 [8] N. Guttenberg and N. Goldenfeld, Friction factor of two-dimensional rough-boundary turbulent soap film flows, *Phys. Rev. E* **79**, 065306 (2009).
 [9] Y. Pomeau, Front motion, metastability and subcritical bifurcations in hydrodynamics, *Physica D* **23**, 3 (1986).
 [10] H. Hinrichsen, Non-equilibrium critical phenomena and phase transitions into absorbing states, *Adv. Phys.* **49**, 815 (2000).
 [11] P. Manneville, On the transition to turbulence of wall-bounded flows in general, and plane Couette flow in particular, *Eur. J. Mech. B Fluids* **49**, 345 (2015).
 [12] P. Manneville, Transition to turbulence in wall-bounded flows: Where do we stand? *Mechanical Engineering Reviews* **3**, 15-00684 (2016).

- [13] J. Nikuradse, Strömungsgesetze in rauhen rohren, in *Forschungsheft auf dem Gebiete des Ingenieurwesens*, VDI-Forschungsheft 361 (VDI-Verlag, Rauhen Rohren, 1933) [English translation: “Laws of flow in rough pipes”, NACA Technical Memorandum 1292 (1950)].
- [14] K. A. Flack, M. P. Schultz, and W. B. Rose, The onset of roughness effects in the transitionally rough regime, *Int. J. Heat Fluid Fl.* **35**, 160 (2012).
- [15] N. Agrawal, G. H. Choueiri, and B. Hof, Transition to Turbulence in Particle Laden Flows, *Phys. Rev. Lett.* **122**, 114502 (2019).
- [16] W. Hogendoorn and C. Poelma, Particle-Laden Pipe Flows at High Volume Fractions Show Transition Without Puffs, *Phys. Rev. Lett.* **121**, 194501 (2018).
- [17] T. S. Lo and J. Koplik, Suspension flow and sedimentation in self-affine fractures, *Phys. Fluids* **24**, 053303 (2012).
- [18] E. Skjetne, A. Hansen, and J. Gudmundsson, High-velocity flow in a rough fracture, *J. Fluid Mech.* **383**, 1 (1999).
- [19] M. Wang, Y.-F. Chen, G.-W. Ma, J.-Q. Zhou, and C.-B. Zhou, Influence of surface roughness on nonlinear flow behaviors in 3D self-affine rough fractures: Lattice Boltzmann simulations, *Adv. Water Resour.* **96**, 373 (2016).
- [20] L. Zou, L. Jing, and V. Cvetkovic, Shear-enhanced nonlinear flow in rough-walled rock fractures, *Int. J. Rock Mechanics Mining Sciences* **97**, 33 (2017).
- [21] S. Briggs, B. W. Karney, and B. E. Sleep, Numerical modeling of the effects of roughness on flow and eddy formation in fractures, *J. Rock Mechanics Geotechnical Engineering* **9**, 105 (2017).
- [22] H. J. Seybold, H. A. Carmona, F. A. L. Filho, A. D. Araújo, F. N. Filho, and J. S. Andrade, Flow through three-dimensional self-affine fractures, *Phys. Rev. Fluids* **5**, 104101 (2020).
- [23] C. Mei and J.-L. Auriault, The effect of weak inertia on flow through a porous medium, *J. Fluid Mech.* **222**, 647 (1991).
- [24] D. Lo Jacono, F. Plouraboué, and A. Bergeon, Weak-inertial flow between two rough surfaces, *Phys. Fluids* **17**, 063602 (2005).
- [25] E. Bouchaud, Scaling properties of cracks, *J. Phys.: Condens. Matter* **9**, 4319 (1997).
- [26] J. Feder, *Fractals*, Physics of Solids and Liquids, 1st ed. (Springer, New York, 2013).
- [27] A.-L. Barabási and H. E. Stanley, *Fractal Concepts in Surface Growth* (Cambridge University Press, Cambridge, England, 1995).
- [28] D. Bonamy, L. Ponsot, S. Prades, E. Bouchaud, and C. Guillot, Scaling Exponents for Fracture Surfaces in Homogeneous Glass and Glassy Ceramics, *Phys. Rev. Lett.* **97**, 135504 (2006).
- [29] A. Neuville, R. Toussaint, and J. Schmittbuhl, Hydrothermal coupling in a self-affine rough fracture, *Phys. Rev. E* **82**, 036317 (2010).
- [30] Y. Méheust and J. Schmittbuhl, Scale effects related to flow in rough fractures, *Pure appl. geophys.* **160**, 1023 (2003).
- [31] M. Mortensen and K. Valen-Sendstad, Oasis: A high-level/high-performance open source Navier–Stokes solver, *Comput. Phys. Commun.* **188**, 177 (2015).
- [32] See Supplemental Material at <http://link.aps.org/supplemental/10.1103/PhysRevResearch.4.033086> for details on flow geometry, mesh generation, numerical scheme, simulation protocol, and some basic observations of the aperture and velocity fields.
- [33] M. Chantry, L. S. Tuckerman, and D. Barkley, Universal continuous transition to turbulence in a planar shear flow, *J. Fluid Mech.* **824**, R1 (2017).
- [34] S. Bottin and H. Chaté, Statistical analysis of the transition to turbulence in plane couette flow, *Eur. J. Mech. B* **6**, 143 (1998).
- [35] X. Xiong, J. Tao, S. Chen, and L. Brandt, Turbulent bands in plane-Poiseuille flow at moderate Reynolds numbers, *Phys. Fluids* **27**, 041702 (2015).
- [36] C. C. Lin, On the stability of two-dimensional parallel flows. III. stability in a viscous fluid, *Quarterly Appl. Math.* **3**, 277 (1946).
- [37] S. Gomé, L. S. Tuckerman, and D. Barkley, Statistical transition to turbulence in plane channel flow, *Phys. Rev. Fluids* **5**, 083905 (2020).
- [38] It should be mentioned that in the directed percolation universality class, where this transition is expected to belong for $A = 0$, the actual critical point is expected to be at a Re very slightly higher than Re_{\times} [4,10].
- [39] M. Thakkar, A. Busse, and N. Sandham, Direct numerical simulation of turbulent channel flow over a surrogate for Nikuradse-type roughness, *J. Fluid Mech.* **837**, R1 (2018).
- [40] T. Ishida, G. Brethouwer, Y. Duguet, and T. Tsukahara, Laminar-turbulent patterns with rough walls, *Phys. Rev. Fluids* **2**, 073901 (2017).
- [41] A. Busse and N. D. Sandham, Parametric forcing approach to rough-wall turbulent channel flow, *J. Fluid Mech.* **712**, 169 (2012).
- [42] J. S. Andrade, U. Costa, M. Almeida, H. Makse, and H. Stanley, Inertial Effects on Fluid Flow through Disordered Porous Media, *Phys. Rev. Lett.* **82**, 5249 (1999).